Persistent currents with non-quantized angular momentum

A. Muñoz Mateo[1], A. Gallemí[1,2], M. Guilleumas[1,2], and R. Mayol[1,2]
[1] *Departament d'Estructura i Constituents de la Matèria, Facultat de Física, Universitat de Barcelona, Martí i Franquès, 1, E–08028 Barcelona, Spain*
[2] *Institut de Nanociència i Nanotecnologia (IN²UB), Universitat de Barcelona*

We analyze the generation of persistent currents in Bose-Einstein condensates of ultracold gases confined in a ring. This phenomenon has been recently investigated in an experiment [Nature **506**, 200 (2014)], where hysteresis loops have been observed in the activation of quantized persistent currents by rotating weak links. In this work, we demonstrate the existence of 3D stationary currents with non-quantized angular momentum. They are generated by families of solitary waves that show a continuous variation in the angular momentum, and provide a bridge between different winding numbers. We show that the size of hysteresis loops is determined by the range of existence within the weak link region of solitary waves which configure the energy barrier preventing phase slips. The barrier vanishes when the critical rotation leads winding numbers and solitonic states to a matching configuration. At this point, Landau and Feynman criteria for phase slips meet: the fluid flow reaches the local speed of sound, and stationary vortex lines (which are the building blocks of solitons) can be excited inside the system.

PACS numbers: 03.75.Lm,67.85.De,67.85.Lm,05.30.Jp

I. INTRODUCTION

Persistent currents are one of the striking phenomena associated to superfluidity. In charged systems, electric currents flowing without dissipation along superconductor loops are due to the superfluid flow of Bose-condensed Cooper pairs, and have found an extensive field of applications since the prediction of SQUIDs [1]. In neutral systems, persistent currents have been observed since the early experiments with superfluid liquid helium (see Ref. [2] and references therein), and have experimented a revival with the advent of Bose-Einstein condensation of ultracold gases. Multiply connected geometries have allowed the generation of long-life currents in Bose-Einstein condensates (BECs) [3–5], paving the way for atomtronic devices.

The effect of a rotating external potential producing a depletion in the density (weak link) has been theoretically and experimentally addressed in rings of ultracold atomic gases [4, 6–8]. The rotating weak link drags the superfluid into a moving state once the resistance of the system to generate excitations has been overcome. Whether superfluid excitations are triggered by reaching the speed of sound, according to Landau criterion, or by vortex nucleation, following Feynman criterion, has yet to be elucidated [7]. Experimental works (see Ref. [9] and references therein) point out that vortices are responsible of the activation of persistent currents in a ring. Phase slips seem to be originated by the transit of a vortices towards the inner (outer) edge of the system [10], producing the increase (decrease) up to one unit in the winding number.

In Ref. [9] a hysteresis loop has been observed in the generation of quantized persistent currents by means of a rotating weak link. A 3D ring of Bose-condensed ^{23}Na atoms was prepared in a stationary state with winding number 0 (1), and the frequency Ω_c^+ (Ω_c^-) at which the winding number changes to 1 (0) was measured. The size of the hysteresis loop, i.e. the difference $(\Omega_c^+ - \Omega_c^-)$, was compared with numerical results obtained by solving the 3D Gross-Pitaevskii equation (GPE), showing a big discrepancy. As the intensity of the link decreases, the size of the loop becomes considerably smaller in the experiment than in the numerics. The reason adduced for the difference points to a dissipation mechanism, but a complete explanation has still not been given.

Hysteresis is a phenomenon intimately linked to systems presenting multiple local energy minima separated by energy barriers that must be overcome when driving the system from one minimum to the other [11]. The final state depends on the path followed in the dynamical evolution searching for equilibrium states. For superfluids in a ring, it is well known that local energy minima correspond to states with different winding number [12]. However, neither the exact nature of the states lying on the barrier nor their stability have been shown yet, although it has been hypothesized that unstable states separate adjacent winding numbers.

In this work we demonstrate the existence of stationary states with non-quantized angular momentum in 3D rings. These states are solitary waves that fill the gap of angular momentum between winding numbers. Among such solitonic states, there exist dynamically stable configurations that can support long-life currents. In addition, we show how the rotating weak link provides common features of solitary waves to winding number states. In doing so, the size of hysteresis loops can be determined by the range of existence of solitary waves within the weak link region. Solitonic states configure the energy barrier preventing phase slips and meet a family of winding number states when the barrier vanishes. This fact indicates that Landau and Feynman criteria may also match. The former stablishes that phase slips are produced when the fluid flow reaches the local speed of sound, at the end of a winding number family of station-

ary solutions. But this is also in agreement with Feynman criterion, which states that phase slips appear when vortex lines can be excited inside the system, as it occurs at the end of a solitonic family of steady states.

II. MODEL

We will consider BECs in a ring-shaped geometry (torus in 3D) of radius R rotating at frequency Ω within the mean-field regime. Stationary states $\Psi(\mathbf{r},t) = \psi(\mathbf{r})e^{-i\mu t/\hbar}$ fulfill the time-independent GPE (in the co-moving frame) with chemical potential μ:

$$\left(-\frac{\hbar^2}{2m}\nabla^2 - \Omega\hat{L}_z + V(\mathbf{r}) + g|\psi|^2\right)\psi = \mu\psi\,, \qquad (1)$$

where $g = 4\pi\hbar^2 a/m$ defines the interaction strength as a function of the s-wave scattering length a, and the external potential $V(\mathbf{r})$ includes harmonic trapping $V_{trap}(\mathbf{r}) = m\omega_z^2 z^2/2 + m\omega_\perp^2(r_\perp - R)^2/2$, with $r_\perp^2 = x^2 + y^2$, and a weak link $U_{wl}(\mathbf{r}) = U_0\exp[-2\,(R(\theta-\theta_0)/w_\theta)^2]$ along the azimuthal coordinate $\theta = \arctan(y/x)$. The angular momentum operator is defined by $\hat{L}_z = -i\hbar\,\partial_\theta$, and the energy can be calculated by $E[\psi] = \int d\mathbf{r}\left\{|(-i\hbar\nabla - m\boldsymbol{\Omega}\times\mathbf{r})\psi|^2/2m + V|\psi|^2 + g|\psi|^4/2\right\}$.

Persistent currents can be supported by states with integer winding number q, quantized angular momentum per particle $\langle\hat{L}_z\rangle/N = \hbar q$, and constant density along θ, that is

$$\Psi_q(\mathbf{r},t) = e^{-i\mu t/\hbar}\psi_q(z,r_\perp)\,e^{iq\theta}\,. \qquad (2)$$

In addition, persistent currents can also be provided by solitonic states, which present non-quantized angular momentum and produce density dips along the ring

$$\Psi_\kappa(\mathbf{r},t) = e^{-i\mu t/\hbar}\psi_\kappa(z,r_\perp,\theta)\,e^{i\kappa\theta}\,, \qquad (3)$$

where κ, a real number, plays the role of a quasimomentum (see below).

III. 1D RINGS

This framework can be easily visualized in 1D rings. Without weak link, the lowest-energy states for a given angular momentum, or *yrast* states, have been identified as solitary waves connecting states with different winding numbers [13–15]. Assuming that a tight transverse harmonic trap enforces a 1D geometry, and using units of $E_R = \hbar^2/mR^2$, the dimensionless 1D version of Eq. (1) without external potential reads

$$\frac{1}{2}\left(-i\partial_\theta - \hat{\Omega}\right)^2\psi + \hat{g}|\psi|^2\psi = \hat{\mu}\psi, \qquad (4)$$

where $\hat{\mu} = \mu/E_R + \hat{\Omega}^2/2$, $\hat{\Omega} = \hbar\Omega/E_R$, $\hat{g} = 2aRN/a_\perp^2$, and $a_\perp = \sqrt{\hbar/m\omega_\perp}$ is the characteristic length of the transverse trap. Among the analytical solutions of Eq. (4), a dark soliton moving with linear velocity v_s along the ring is given by Eq. (3) with

$$\psi_\kappa(\theta) = \sqrt{\frac{\mu}{\hat{g}E_R}}\left[i\beta + \gamma\tanh\left(\gamma\sqrt{\frac{\mu}{E_R}}\,\theta\right)\right]\,, \qquad (5)$$

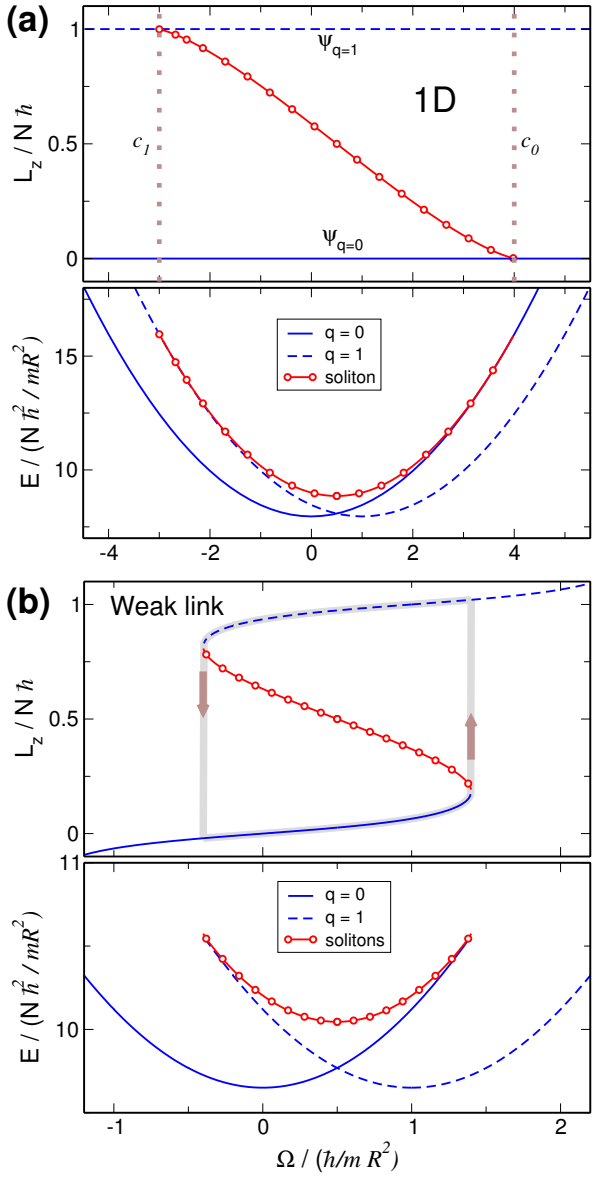

FIG. 1. Soliton connection between winding-number states in a 1D ring for condensates with $\hat{g} = 100$. Only winding numbers 0 and 1 are considered, without (a) and with (b) external weak link of depth $U_{wl} = 0.56\,\mu$ and width $w_\theta = R$ along the angular coordinate. For each case, angular momentum per particle is shown above and energy per particle below. The thick dotted lines of the top graph (a) indicate the values of the speed of sound, c_0 and c_1, relative to the winding number state 0 (right) and 1 (left). The hysteresis loop is displayed in (b) by thick gray lines and arrows.

where $\gamma^2+\beta^2=1$, $\beta=v_s/c$, $c=\sqrt{\mu/m}$ is the speed of sound, and $\hbar\kappa/mR=\Omega R-v_s$. As can be seen in Fig. 1(a), solitons (open circles), given by Eqs. (3) and (5), connect states $\psi_q(\theta)\propto e^{iq\theta}$ having consecutive winding phases (solid and dashed lines).

By producing localized density depletions in the ring, a single soliton induces a phase jump $\Delta S=2\arccos\beta$ in the condensate wave function [16]. These phase jumps need to be counterbalanced by background currents around the torus, with angular speed $\kappa=-q-\Delta S/2\pi$, to ensure a single-valued order parameter whenever a closed loop is followed. The resulting flow carries angular momentum per particle, $\langle\hat{L}_z\rangle/N\hbar=-\beta\gamma/\pi-\kappa+(\Delta q-1)/2$, which takes continuous values in the range between integer winding numbers q and $q+\Delta q$, with $\Delta q=\pm1$. The velocity of moving solitons v_s cannot exceed the speed of sound c, at which nonlinear soliton excitations transform into linear sound waves traveling on a winding number state. Therefore this speed limit bounds the range of existence of solitonic solutions. Provided that solitonic states can show dynamical stability [14], their associated flows will appear as persistent currents. We will see that there exist the counterpart of these states in multidimensional systems.

A. Weak link

The presence of a rotating weak link introduces variations in the density profile that give rise to phase jumps, and, like in solitons, background currents are generated in order to compensate such jumps. Fig. 1(b) displays our results obtained from the numerical solution of Eq. (4) for a system with $\hat{g}=100$, and weak link of depth $U_{wl}=0.56\,\mu$ and width $w_\theta=R$. As can be seen, and contrary to the case without weak link, both winding number and solitonic states show variations in the angular momentum with the rotation rate. This effect can be deduced from the expression for the current density $\mathbf{j}(\mathbf{r},t)=\rho(\hbar\nabla S/m-\mathbf{\Omega}\times\mathbf{r})$, expressed in terms of density ρ and phase S of the order parameter $\Psi(\mathbf{r},t)=\sqrt{\rho(\mathbf{r},t)}e^{iS(\mathbf{r},t)}$. Defining the velocity as $v=j/\rho$ we get $v(\theta)=\hbar(\partial_\theta S(\theta)-\hat{\Omega})/mR$ for the 1D case. Solving for the phase gradient and integrating along the whole ring we obtain

$$2\pi q=2\pi\hat{\Omega}+\frac{mR}{\hbar}\oint d\theta\, v(\theta)\,, \qquad (6)$$

where, due to the single-valuedness of the order parameter, we used $S(\theta=2\pi)-S(\theta=0)=2\pi q$. Whenever the dimensionless angular rotation $\hat{\Omega}$ takes integer values, it is possible to look for static states having $v(\theta)=0$. Instead, stirring the system at non-integer $\hat{\Omega}$ values imposes a non-vanishing velocity, hence phase gradients.

As a consequence of the weak link, which breaks the rotational symmetry of the system, a gap is opened in the energy spectrum of winding numbers [11]. Our numerical results, displayed in Fig. 1(b), quantify the qualitative analysis of this fact made previously in the literature. As can be seen, swallow tails are developed in the presence of a weak link, cutting the otherwise continuous curves traced by winding numbers in Fig. 1(a). Generating solitons at the weak link position is energetically more favorable than at higher-density regions. For weak link extents w_θ greater than the healing length $\xi=\sqrt{\hbar^2/m\mu}$, a local speed of sound $c(\theta)=\sqrt{g\,n_1(\theta)/m}$ can be defined (n_1 being the azimuthal density), which takes the lowest value at the weak link center. As the speed of sound is a measure of the range of existence of solitonic solutions, this range is reduced inside the low density region, relative to the system without weak link.

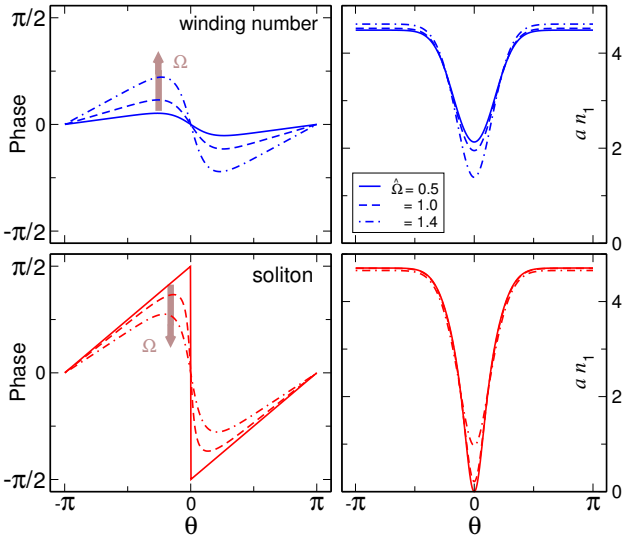

FIG. 2. Phases (left column) and dimensionless azimuthal densities (right column), obtained from numerical solutions of the time-independent 1D GPE (4), corresponding to winding number $q=0$ (above) and solitonic states (below) for the same parameters as in Fig. 1(b), rotating at angular frequencies $\hat{\Omega}=0.5$, 1.0 and 1.4. Thick arrows (on the left column) indicate the sequence of both type of states for increasing Ω, approaching convergence near $\hat{\Omega}=1.4$.

When rotation is introduced, opposite effects can be observed in solitonic and winding-phase states (see Fig. 2). For increasing angular frequency, solitons decrease their angular momentum, whereas winding numbers increase it. In this way, both type of solutions converge at some intermediate value, where the superfluid flow reaches the speed of sound at the weak link. Therefore, the bounds for the existence of solitons are also applicable to states with a winding phase.

Hysteresis loops, as those observed in the experiment [9], can be clearly identified in Fig. 1(b) (thick brown lines and arrows). Distinct from previous analyses, our results are able to measure the size of the energy barrier preventing phase slips. Solitonic states are the responsible of such barrier, occupying stationary points in the energy landscape of the system. The barrier vanishes when

both type of states connect, and it is no longer possible to continue beyond these points by increasing the angular velocity. As a result the system decays to the next lower-energy winding-phase state. When the intensity of the weak link grows, the speed of sound and hysteresis cycle width reduce, and solitons and winding-phase states become energetically closer.

IV. 3D RINGS

In multidimensional systems, the 1D picture outlined before is reproduced: solitons are the stationary states making the connection between winding numbers and building the energy barrier separating them. In addition, dimensionality allows the emergence of novel solitonic states and introduces new issues concerning their stability. It was demonstrated in Ref. [17] that different transverse standing waves can be excited in straight-channeled superfluids. A dark soliton possesses the simplest structure among such standing waves, and it is a dynamically stable configuration for small values of the chemical potential, when no other transverse states can be excited. But more complex configurations containing vortex lines are also possible. They emerge at higher values of the chemical potential, and thus higher densities, and cause the dark soliton to turn into a dynamically unstable configuration. The stable state is then the solitonic vortex [18], i.e. the state containing a single vortex line, which have been recently observed in elongated geometries [19, 20]. It is worth to mention that also in toroidal systems, off-centered vortex lines (solitonic vortices) have been observed [8] in the density regions of the condensate.

We have numerically solved the 3D GPE (1), by using the Newton method, in order to find steady states supporting stationary currents in toroidal condensates with typical experimental parameters. Fig. 3(a) displays data for a regime where, apart from winding number states, two types of solitary waves are possible: dark solitons and solitonic vortices. Our results show that 3D toroidal condensates support standing waves equivalent to those found in straight channels, and follow the same energy criterion for their bifurcation. At the scale of Fig. 3(a), the energies of dark solitons and solitonic vortices are indistinguishable, and the main difference is their range of existence. While dark solitons there exist only for values of the angular momentum per particle around $(q+1/2)\hbar$, solitonic vortices extend into the regions approaching winding numbers. This approach is mediated by the two different branches of Fig. 3(a) that are represented by means of lines with right and left pointing triangles, along with two characteristic density isocontours. The former branch is connecting with the winding number $q = 0$, and consists of vortices that produce flows rotating in the same direction as Ω, while the latter connects with the winding number $q = 1$ and contains counterrotating vortices (antivortices).

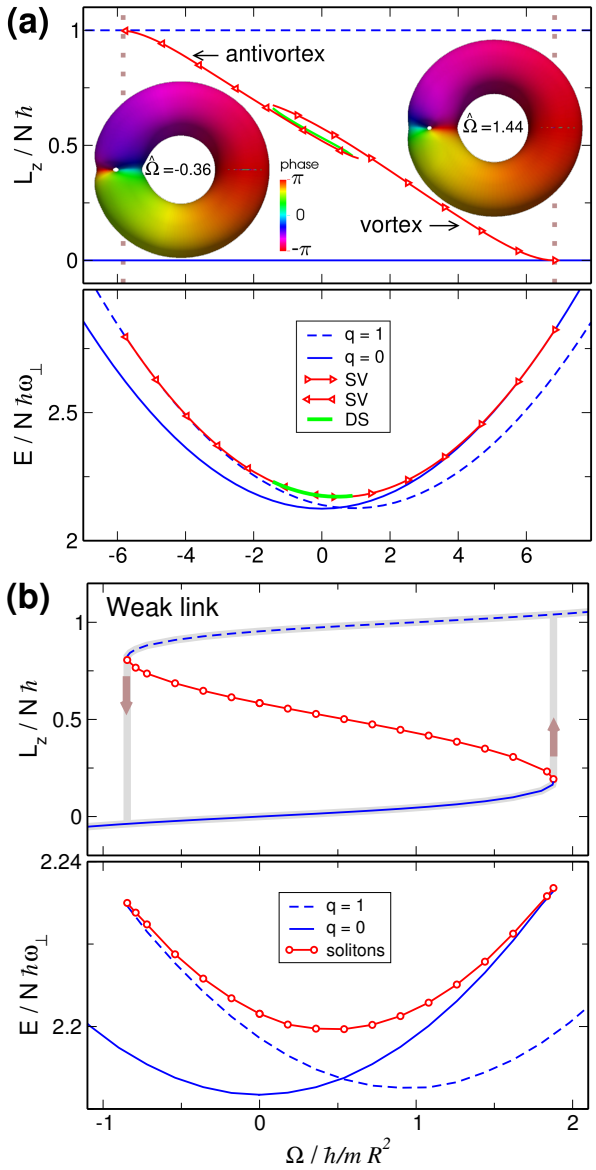

FIG. 3. Same as Fig. 1 for a 3D system, showing numerical results of time-independent 3D GPE (1) for condensates containing 5.3×10^4 atoms of ^{23}Na in an isotropic harmonic trap with $\omega = 2\pi \times 100$ Hz centered at $R = 6\,a_\perp$. Two solitary waves can be excited in the absence of weak link (a), solitonic vortex (SV) and dark soliton (DS), whereas only a DS is possible at the center of a weak link (b) with depth $U_{wl} = 0.5\,\mu$ and width $w_\theta = 0.6\,R$. The insets represent density isocontours (at 5% of maximun density), coloured by phase, of SVs belonging to two separated branches containing either vortices or antivortices. The external diameter of the tori is $17\,a_\perp$.

It is noteworthy that hysteresis is also present in solitonic vortex states, since the two mentioned branches are separated by an energy barrier occupied by dark solitons (thick green line in Fig. 3(a)). This energy difference between solitonic states is responsible of their stability properties. As shown in Fig. 4, dark solitons decay into

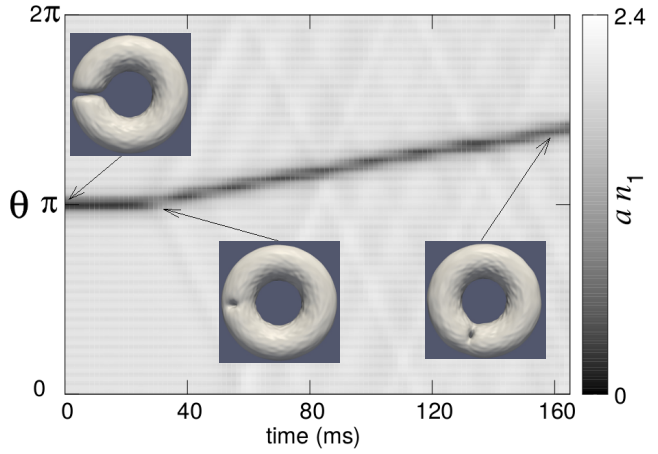

FIG. 4. Evolution in real time, obtained by solving the 3D time-dependent GPE, of a dark soliton state, with the same parameters as in Fig. 3, after an initial Gaussian perturbation. Dimensionless azimuthal density $an_1(\theta)$ is plotted as a function of time. Density isocontours (at 5% of maximum density) are showed for times (from left to right) 0, 32 and 160 ms.

solitonic vortices, which are dynamically stable states. To show it, we have evolved in real time a dark soliton state made of 5.3×10^4 atoms of ^{23}Na in an isotropic harmonic trap with $\omega = 2\pi \times 100$ Hz centered at $R = 6\,a_\perp$. After adding Gaussian noise to the initial stationary solitonic state, we observe that it survives during, approximately, the first 20 ms of the simulation, before decaying into another solitary wave, a solitonic vortex, and emitting phonons. The subsequent evolution shows the motion of the emergent soliton with a different inertial mass than the initial state [21, 22].

As in the 1D case, multidimensional solitons can exist only while their velocity around the torus is lower than the speed of sound. For isotropic harmonic trapping, the speed limit is given by the azimuthal speed of sound $c(\theta)$ that can be calculated by [23]

$$c(\theta) = \sqrt{\frac{\mu^2(\theta) - (\hbar\omega_\perp)^2}{2m\,\mu(\theta)}}\,. \qquad (7)$$

In Fig. 3(a), the thick dotted lines represent the values given by Eq. (7). The manifest agreement with numerical solutions of GPE (lines with open triangles), permits Eq. (7) to be employed for predicting the range where solitons exist and hence for measuring the size of hysteresis loops.

A. Weak link

The presence of the weak link introduces new effects in 3D systems. The density depletion reduces not only the local speed of sound, as in 1D systems, but also the local energy available for transverse excitations. As a result, some solitonic states that can be excited in regions with homogeneous density could not survive at the weak link. This is exactly the case represented in Fig. 3(b), where solitonic vortices are excluded from the weak link region, and only dark solitons can be excited inside. As rotation starts, non-null currents are generated in winding-phase states. In analogy with the Meissner effect, the system produces a counter flow inside the weak link region in order to exclude the vorticity field induced by rotation. In a multidimensional system, a vortex-antivortex pair produces such a flow [24, 25]. The rotating weak link leads surface modes to enter into the torus by nucleating a vortex dipole along the radial direction [6, 7]. This dipole yields a phase jump which is opposite to the background flow and has the required value for keeping a winding phase. The phase jump grows with increasing angular rotation, up to a critical point where the flow velocity inside the weak link reaches the local speed of sound, and no further increase is allowed. At this point, which is also the end of the trajectory for solitons inside the weak link, the localized phase jump vanishes and a phase slip is produced. This effect is due to the dispersion curve of vortex dipoles [26], which transform into phonons at low momentum p, that is to say, when $E/p \to c$. As a consequence, the size of hysteresis loops in 3D rings is determined by the range of existence of solitonic solutions, and this range is bounded by the local speed of sound $c(\theta)$.

Figure 5 shows the approach to the critical angular frequency followed by winding number states (upper graph in the figure) and solitons (lower) for a torus with the same parameters as before. At intermediate rotation rates, $\hat{\Omega} = 0.5$, a dark soliton has angular momentum per particle $\langle L_z\rangle/N\hbar = 0.5$, whereas the winding number $q = 0$ produces a small current, represented on the figure by an almost imperceptible gradient phase. However, as can be seen in the isocontours situated on the right at Fig. 5, at the rotation rate $\hat{\Omega} = 1.87$, close to the critical frequency, the differences between solitonic and winding numbers begin to disappear, and the converging process finishes with a phase slip to winding number $q = 1$, when the local speed of sound is reached.

V. CONCLUSIONS

We have studied the generation of persistent currents by means of rotating weak links in 3D Bose-Einstein condensates confined in a torus. We demonstrate the existence of persistent currents with non-quantized angular momentum supported by stationary states that include solitary waves. They are equivalent to the solitonic waves found in straight channels [17], and follow the same energy criterion for their bifurcation. In the presence of a rotating weak link, stationary solitons lying at the weak link give the lowest height of the energy barrier separating winding numbers and preventing phase slips. We show that the energy barrier vanishes when the angular

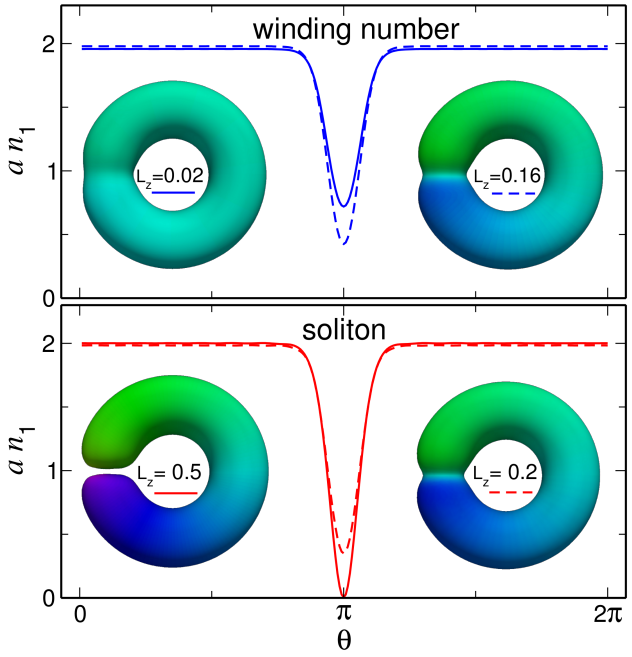

FIG. 5. Density isocontours (5% of maximum density) of winding number $q = 0$ (above) and solitonic (below) states, obtained by solving the time-independent 3D GPE 1, in 3D condensates with the same trap and rotating weak link as those of Fig. 3. Angular momentum per particle $\langle L_z\rangle/N\hbar$ is indicated in the inner part of the tori. The angular frequencies considered are $\hat{\Omega} = 0.5$ (left) and $\hat{\Omega} = 1.87$ (right), the latter near the critical frequency where states approach $\langle L_z\rangle/N\hbar = 0.18$. Background graphs show the dimensionless density $an_1(\theta)$, after integrating along $(z, r_\perp)$. Colours represent the phase following the colour map of Fig. 3.

frequency makes such solitons to move at the local speed of sound. At this rotation rate, the families of winding numbers and solitons converge, in such a way that time-independent states belonging to these families do not exist for a faster rotation, and a phase slip is produced.

Our results point out that the size of the hysteresis loops observed in Ref. [9] is characterized by the convergence process between winding numbers and solitons. This connection allows to identify, at the end of the hysteresis loop, both stationary vortex lines (making solitonic states), and phonons (traveling at the speed of sound on winding number states). This fact indicates that Feynman and Landau criteria for the generation of phase slips meet at the connection point.

However, the controversy about the different sizes of hysteresis loops given by Gross-Pitaevskii theory and experiments remains. As long as we are dealing with quantum mechanical systems, quantum tunneling processes can be considered in order to get phase slips [27]. It is not necessary for the system to wait for changing its angular momentum up to the configuration where the energy barrier vanishes. These calculations are beyond the aim of the present work and will be reported elsewhere [28].

[1] R. C. Jaklevic, J. Lambe, A. H. Silver and J. E. Mercereau, Phys. Rev. Lett. **12**, 159 (1964).
[2] E. Hoskinson, Y. Sato, I. Hahn and R. E. Packard, Nature Physics **2**, 23 (2006).
[3] C. Ryu, M. F. Andersen, P. Cladé, V. Natarajan, K. Helmerson and W. D. Phillips, Phys. Rev. Lett. **99**, 260401 (2007).
[4] A. Ramanathan, K. C. Wright, S. R. Muniz, M. Zelan, W. T. Hill, C. J. Lobb, K. Helmerson, W. D. Phillips and G. K. Campbell, Phys. Rev. Lett. **106**, 130401 (2011).
[5] S. Moulder, S. Beattie, R. P. Smith, N. Tammuz and Zoran Hadzibabic, Phys. Rev. A **86**, 013629 (2012).
[6] F. Piazza, L. A. Collins and A. Smerzi, Phys. Rev. A **80**, 021601(R) (2009).
[7] F. Piazza, L. A. Collins and A. Smerzi, J. Phys. B: At. Mol. Opt. Phys. **46** 095302 (2013).
[8] K. C. Wright, R. B. Blakestad, C. J. Lobb, W. D. Phillips and G. K. Campbell, Phys. Rev. Lett. **110**, 025302 (2013).
[9] S. Eckel, J. G. Lee, F. Jendrzejewski, N. Murray, C. W. Clark, C. J. Lobb, W. D. Phillips, M. Edwards and G. K. Campbell, Nature, **506**, 200 (2014). Phys. Rev. Lett. **106**, 130401 (2011).
[10] M. Abad, M. Guilleumas, R. Mayol, F. Piazza, D. M. Jezek and A. Smerzi, Europhys. Lett. **109**, 40005 (2015).
[11] E. J. Mueller, Phys. Rev. A **66**, 063603 (2002).
[12] F. Bloch, Phys. Rev. A **7**, 2187 (1973).
[13] B. Mottelson, Phys. Rev. Lett. **83**, 2695 (1999).
[14] R. Kanamoto, L. D. Carr and M. Ueda, Phys. Rev. A **79**, 063616 (2009).
[15] A. D. Jackson, J. Smyrnakis, M. Magiropoulos and G. M. Kavoulakis, Europhys. Lett. **95** 30002 (2011).
[16] P. Pitaevskii and S. Stringari, *Bose-Einstein condensation* (Oxford University Press, New York, 2003).
[17] A. Muñoz Mateo and J. Brand, Phys. Rev. Lett. **113**, 255302 (2014).
[18] J. Brand and W. P. Reinhardt, J. Phys. B: At. Mol. Opt. Phys. **34**, 4 (2001).
[19] M. J.H. Ku, W. Ji, B. Mukherjee, E. Guardado-Sanchez, L. W. Cheuk, T. Yefsah and M. W. Zwierlein, Phys. Rev. Lett. **113**, 065301 (2014).
[20] S. Donadello, S. Serafini, M. Tylutki, L. P. Pitaevskii, F. Dalfovo, G. Lamporesi and Gabriele Ferrari, Phys. Rev. Lett. **113**, 065302 (2014).
[21] R. G. Scott, F. Dalfovo, L. P. Pitaevskii and S. Stringari, Phys. Rev. Lett. **106**, 185301 (2011).
[22] R. Liao and J. Brand, Phys. Rev. A **83**, 041604(R) (2011).

[23] A. Muñoz Mateo and V. Delgado, Phys. Rev. A **75**, 063610 (2007).
[24] S. J. Woo and Y.-W. Son, Phys. Rev. A **86**, 011604(R) (2012).
[25] R. Dubessy, T. Liennard, P. Pedri and H. Perrin, Phys. Rev. A **86**, 011602(R) (2012).
[26] C. A. Jones and P. H. Roberts, J. Phys. A: Math. Gen. **15**, 2599 (1982).
[27] J. A. Freire, D. P. Arovas and H. Levine, Phys. Rev. Lett. **79**, 5054 (1997).
[28] A. Muñoz Mateo, A. Gallem í, M. Guilleumas, R. Mayol and J. Gomis. To be published.